Optical and EPR investigations of Np^{4+} in single crystals of $ZrSiO_4$

I. Poirot, W. Kot, G. Shalimoff, and N. Edelstein
Materials and Chemical Sciences Division, Lawrence Berkeley Laboratory, University of California, Berkeley, California 94720 and Department of Chemistry, University of California, Berkeley, California 94720

M. M. Abraham, C. B. Finch, and L. A. Boatner
Solid State Division, Oak Ridge National Laboratory, Oak Ridge, Tennessee 37831-6061
(Received 1 June 1987)

Polarized optical spectroscopy has been used to investigate the electronic structure of tetravalent neptunium incorporated as a dilute impurity in single crystals of the tetragonal host $ZrSiO_4$. Thirty-one levels were assigned from 30 intense polarized optical transitions and used to obtain a fit to a parametric Hamiltonian to within an rms deviation of 34 cm^{-1}. Thirteen other levels with comparable intensities and good polarization characteristics were observed. Inclusion of these levels using the parameters from the 31-level fit, however, resulted in an increase of the rms deviation to approximately 100 cm^{-1}. The EPR spectra of the ground state of Np^{4+}:$ZrSiO_4$ were measured and fit to an axial spin Hamiltonian to obtain the parameters: $|g_{\parallel}|=0.8\pm0.6$, $|g_{\perp}|=2.59\pm0.02$, $A=-2400\pm1200$ MHz, and $B=4750\pm30$ MHz. These results are consistent with the calculated Γ_6 ground state.

I. INTRODUCTION

High-resolution optical spectra of trivalent lanthanide and actinide ions in single crystals have been obtained for over 30 years. The parametric theory used to interpret these spectra has been quite successful.[1] However, the same theory applied to tetravalent ions such as U^{4+} results in fits much worse than found for the trivalent ions.[2] Few optical spectral studies have been published for tetravalent f^n ions in single crystals with atomic number greater than 92 because of the radioactivity of these nuclei and the associated problems. As the atomic number (Z) increases, the actinide ions become more lanthanide-like. This leads to the expectation that the parametric theory which works satisfactorily for the trivalent f^n ions should be more successful for the higher Z tetravalent ions. In order to obtain further information on this point, we present here the optical spectrum of Np^{4+} diluted in $ZrSiO_4$ and analyze the assigned energy levels in terms of a parametric Hamiltonian. In addition, the ground state of Np^{4+}:$ZrSiO_4$ has been characterized by its electron paramagnetic resonance (EPR) spectrum.

Investigations of the optical spectra of tetravalent neptunium incorporated as a dilute impurity in the single crystal hosts ThO_2 and $PbMoO_4$ were first reported in 1969.[3,4] Subsequently, optical spectroscopic studies of Np^{4+} in the host single crystal Cs_2NpCl_6 were carried out.[5] In all of these early investigations, assignments were made only to the low-lying levels of Np^{4+}. More recently, optical spectroscopic investigations of Np^{4+} doped into two additional host single crystals have been reported.[6,7] Tetravalent neptunium has been studied as a dilute impurity in $Zr(BD_4)_4$ and 46 levels were assigned in the spectrum and fit to a parametric Hamiltonian with an rms deviation $\sigma=84$ cm^{-1}.[6] Np^{4+} has also been investigated as an impurity in single crystals of $ThSiO_4$. In this case, 29 levels were assigned in the observed spectrum and were fit with an rms deviation $\sigma=47$ cm^{-1}.[7]

$ZrSiO_4$ (zircon) and $ThSiO_4$ belong to an isostructural class of tetragonal crystals that includes $HfSiO_4$, YPO_4, and the heavier lanthanide orthophosphates, vanadates, and arsenates. The metal ion is located at a site of D_{2d} symmetry surrounded by eight oxygen atoms in a dodecahedral array. The S_4 axis of the metal atom site is parallel to the optic axis of the crystal.[8-10] Zr^{4+} has an eight-coordinate ionic radius of 0.84 Å while the eight-coordinated ionic radius of Th^{4+} is 1.05 Å.[11] Thus the crystal-field interaction for an impurity ion is expected to be larger in $ZrSiO_4$ than in $ThSiO_4$. The reported optical spectra of U^{4+} diluted into $ZrSiO_4$ and $ThSiO_4$ single crystals are consistent with this expectation as the spectra of the two systems differ markedly.[12-14] Nevertheless, it is expected that the crystal-field parameters will not vary greatly for two consecutive ions in the periodic table (U^{4+} and Np^4) in the same host crystal. It is with this premise that we have performed the following analysis.

II. EXPERIMENTAL

A. Optical measurements

Single crystals of $ZrSiO_4$ doped with Np^{4+} were grown in platinum crucibles in air using a lithium molybdate ($Li_2O\cdot6MoO_3$) flux. After heating the crystal growth charge to 1350 °C, the growth furnace was slowly cooled (at about 1 °C/h) to 950 °C. The crystal growth procedures have been described in detail elsewhere.[15-17] Crystal growth runs were carried out with doping levels of 0.2 wt. % Np and 2.0 wt. % Np relative to $ZrSiO_4$.

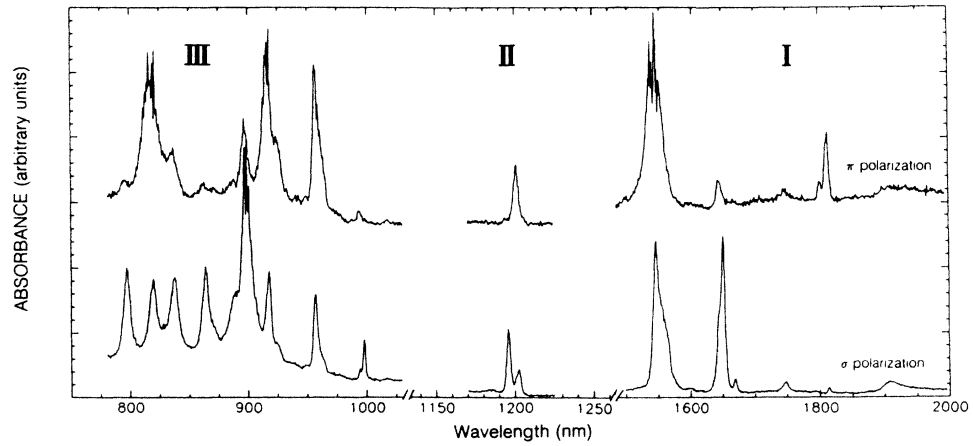

FIG. 1. Polarized absorption spectra of the 1 wt. % Np^{4+}:$ZrSiO_4$ at 4.2 K in the 20 000–7800 Å (2000–780 nm) range.

Single crystals of $ZrSiO_4$ grown with the lower Np doping were well formed and transparent, and a specimen $\sim 2\times 2\times 2$ mm^3 was selected for use in the optical spectroscopic investigations. In the case of the $ZrSiO_4$ crystals with the higher Np doping, although the crystals were larger relative to the lightly doped samples, they exhibited a green color and contained inclusions. Accordingly, it was necessary to prepare the optical samples by cutting thin (~ 0.5 mm) sections with known orientations from the larger "as grown" crystals. The two types of crystals were mounted on slotted copper plates with their optical axis either perpendicular or parallel to the slit, and then sealed in quartz tubes containing a partial pressure of helium gas.

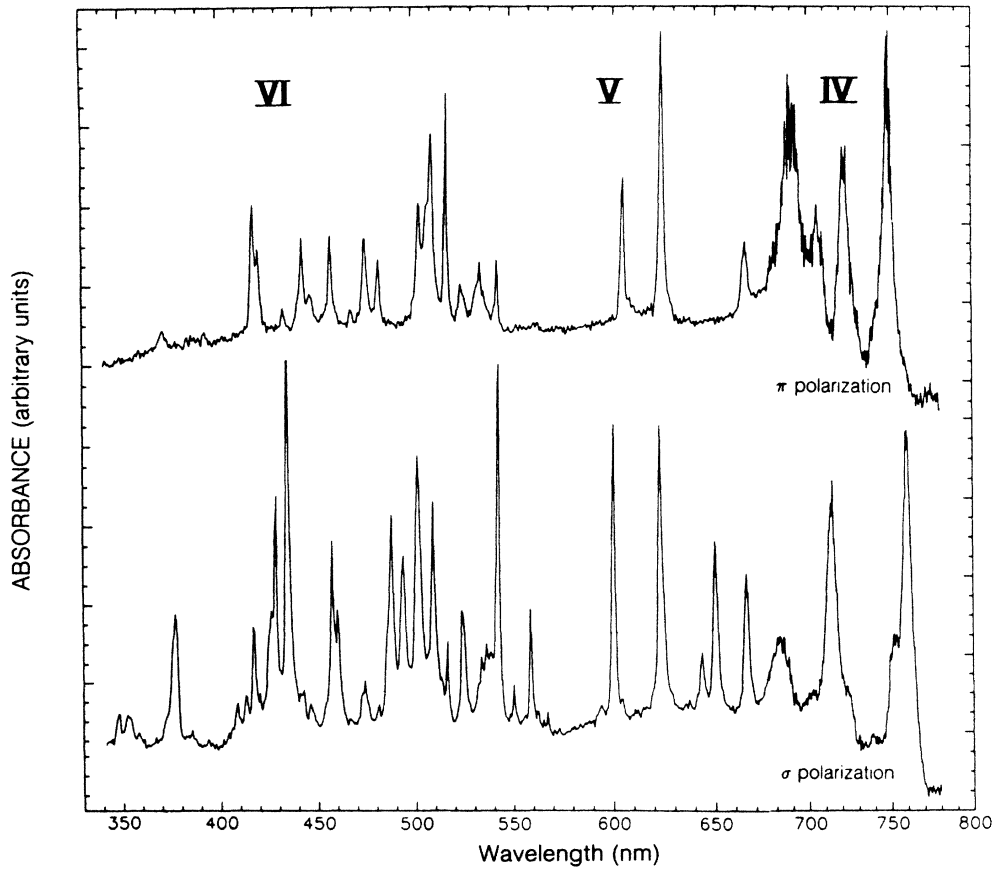

FIG. 2. Polarized absorption spectra of the 1 wt. % Np^{4+}:$ZrSiO_4$ at 4.2 K in the 7800–3400 Å (780–340 nm) range.

The Np concentration for both doping levels was determined by γ ray counting methods. The Np decay [Eq. (1)]

$$^{237}_{93}\mathrm{Np} \xrightarrow[2.14\times10^{6}\ \mathrm{yr}]{\alpha} {}^{233}_{91}\mathrm{Pa} \xrightarrow[27\ \mathrm{day}]{\beta^-} {}^{233}_{92}\mathrm{U} \xrightarrow[1.62\times10^{5}\ \mathrm{yr}]{\alpha} \quad (1)$$

was at equilibrium in these crystals, and the relative intensities of the spectra of multiple γ- and x-ray lines of Pa, U, and Np were compared to a reference with the same geometry (i.e., 1 mg of dissolved Np evaporated on a copper plate and sealed in glass tubing). The high energy (100 to 340 keV) γ- and x-ray lines of ^{233}Pa, which were unaffected by the glass tubing and the crystal, gave measured Np concentrations of approximately 0.1 and 1.0 wt. % for the low and high doping levels of Np in $ZrSiO_4$, respectively.

The optical absorption spectra for both σ and π polarizations were recorded between 20 000 Å and 3500 Å at room, liquid N_2, and liquid He temperatures (see Figs. 1 and 2) using a Cary 17 spectrophotometer. In addition, absorption spectra in the 7600–3500 Å range were taken at 4.2 K with Jarrell-Ash *F*6 and 3.4 m spectrographs. At liquid helium temperature, the observed line widths varied between 15 and 70 cm^{-1}, with the average value being approximately 30 cm^{-1}. Attempts were made to obtain the Zeeman spectra in a magnetic field of 2.7 T at 4.2 K with the magnetic field applied parallel and perpendicular to the optical axis, but no line broadening or splittings were observed. Additionally, no fluorescence was observed in the visible and near infrared (ir) regions and no electronic Raman spectra were detected at 4.2 K for either crystal.

B. EPR measurements

EPR spectra were obtained at 4.2 K and 35 GHz using a Varian E110 microwave resonance spectrometer with an electromagnet that could be rotated about the vertical axis. The maximum obtainable magnetic field was 16 kG. The magnetic-field positions of the EPR transitions were measured by a proton NMR Gaussmeter, and the microwave frequency was determined with an EIP-548 microwave frequency counter.

A single crystal of Np doped $ZrSiO_4$ was selected and oriented in the cylindrical 35 GHz cavity (TE_{011}) so that the applied magnetic field could be rotated in the ac crystallographic plane. All six hyperfine lines for the $I=\frac{5}{2}$ ^{237}Np isotope were observed with **H** perpendicular to the *c* axis of the crystal. These lines moved to higher-field values as the field orientation was rotated toward the crystal *c* axis. Magnetic-field positions were recorded as a function of the magnetic-field orientation at angles where at least three hyperfine lines could be observed (the other lines having shifted above the range of the magnetic field). This corresponded to a rotation of approximately $\pm50°$ about the direction perpendicular to the *c* axis. Additionally, because of problems in positioning the crystal that was encapsulated in polyethylene tubing in the microwave cavity, a $\pm10°$ uncertainty is estimated in the orientation of the plane of magnetic-field rotation relative to the ac plane of the $ZrSiO_4$ crystal.

III. OPTICAL RESULTS

The optical absorption results described above in Sec. II A can be divided into six groups of transitions. Table I lists the wavelengths for the transitions observed with both the dilute and concentrated Np^{4+} doped $ZrSiO_4$ single crystals along with the polarization characteristics, intensities, and assignments for the transitions. For an odd electron system (as in Np^{4+}, $5f^3$) in D_{2d} symmetry, the Kramers degenerate states are classified by the Γ_6 and Γ_7 double-group representations. The selection rules for electric-dipole transitions are: $\Gamma_6 \leftrightarrow \Gamma_7(\mathbf{E}\|\mathbf{c})\pi$ polarization; Γ_6 or $\Gamma_7 \leftrightarrow \Gamma_6$ or $\Gamma_7(\mathbf{E}\perp\mathbf{c})\sigma$ polarization; where **E** is the electric field vector of the incoming radiation and **c** is the S_4 axis of the crystal.[18] From a preliminary calculation described later it was assumed the ground state was of Γ_6 symmetry. The features and details of the six groups of optical transitions are described in the following section.

A. First group (5000–6000 cm^{-1}, 20 000–15 000 Å) (Fig. 1)

Six absorption bands appeared in this range in $ZrSiO_4$ crystals with both Np^{4+} doping levels. This clearly isolated group was assigned to the $^4I_{11/2}$ multiplet which should split in a D_{2d} crystal field into three Γ_6 and three Γ_7 levels. These features became better resolved as the crystals were cooled. Five of the bands showed strong σ or π polarization and could be assigned on this basis. Only a few of the bands exhibited the expected polarization extinction. Generally, the π absorption lines were not accompanied by a σ transition (at 5514, 6072, 6096 cm^{-1}) as permitted by the selection rules. The 17470±10 Å band must be attributed to a transition to a Γ_6 level even though a very weak and broad absorption appears with π polarization.

The weak, broad absorption at about 19 350 Å was only observed at room temperature and gave an indication of the ground term splitting. This peak is separated by 350 cm^{-1} from the 5515 cm^{-1} transition. It has the same π polarization and resulted from the partial population of the first excited Γ_6 level of the $^4I_{9/2}$ manifold at room temperature.

Some other broad, weak lines and shoulders were observed, but they could not be assigned. These features may be due to electronic plus vibronic excitations. Furthermore, particularly in this group, the heavily doped $ZrSiO_4$ crystal showed additional absorption lines as compared to the more dilute crystal. These extra lines were strongly polarized and indicate that an additional site may be present at higher Np concentration levels.

B. Second group (8300–8400 cm^{-1}, 12 500–11 500 Å) (Fig. 1)

Two absorption lines are observed in this range and these were assigned to the $^4F_{3/2}$ state that is split into Γ_6 and Γ_7 levels. Again the Γ_6 to Γ_7 transition is intense for π polarization (at 12 000 Å) for both Np concentrations, but is very weak in σ polarization, and in fact, is barely visible in the dilute Np-doped crystal.

TABLE I. Absorption spectra of Np^{4+}:$ZrSiO_4$.

λ(Å) Conc. crystal	λ(Å) Diluted crystal	Energy (cm^{-1})	Polarization intensity[a]		Assigned representation
1st group					
19 348	19 350	5167	π	*W*(dis. at 4 K)	
19 079	19 150	5240	σ,π	VW&Br.	
18 131	18 140	5514	π	*S*	Γ_7
18 029		5545	π	VW	
17 472	17 472	5723	σ,π weak	*M*	Γ_6
16 692		5989	σ	*M*	
16 506	16 470	6056	σ	*M*	Γ_6
16 465	16 420	6072	π	*M*	Γ_7
15 586	15 520	6500	σ,π	*sh*	
15 456	15 450	6468	σ	*S*	Γ_6
15 391	15 380	6496	π	VS	Γ_7
2nd group					
12 030	12 000	8310	π,σ weak	*M*	Γ_7
11 950	11 930	8366	σ	*M*	Γ_6
3rd group					
10 350	10 350	9659	σ	VW(dis. at 4 K)	
10 175		9825	σ,π	VW&Br.	
9981	9960	10 016	σ	*W*	Γ_6
9936	9920	10 062	π	*W*	Γ_7
9634		10 377	σ,π	*sh*	
9566	9568	10 450	$\sigma,st\pi$	*M*	Γ_7^c
9237	9220	10 823	σ,π	VW,*sh*	
9175	9160	10 896	$\sigma,st\pi$	VS	Γ_7^c
8971	8969	11 147	$st\sigma,\pi$	VS	Γ_6^c
8880		11 258	σ	*sh*	
8640	8615	11 571	σ,π weak	*S*	Γ_6^c
8376	8350	11 935	σ,π weak	*S*	Γ_6
8197	8195	12 196	$\sigma,st\pi$	VS	Γ_7
7974	7930	12 537	σ,π weak	*S*	Γ_6
4th group					
7590	7570	13 188	σ	*S*	Γ_6
7495	7480	13 352	π	*S*	Γ_7
7513		13 306	σ	*sh*	
7243		13 802	σ	VW	
7225	7200	13 861	π	*S*	Γ_7^c
7135	7110	14 036	σ	*S*	Γ_6^c
7061		14 158	π	*M*	Γ_7^c
6904	6870	14 555	π	*S*	Γ_7
6818		14 663	$\sigma,\pi sh$	*W*	
6664	6653	15 014	σ,π	*M*	Γ_7
6511	6502	15 365	σ	*M*	b
6444	6437	15 514	σ	*W*	
6255	6250	15 983	$\pi,\sigma sh$	*S*	Γ_7^c
6240	6235	16 025	σ	*S*	Γ_6^c
5th group					
6064	6057	16 495	π	*M*	Γ_7
6011	6005	16 640	σ	*S*	Γ_6^c
6th group					
5681	5672	17 610	σ	VW	
5630	5654	17 750	σ	VW	
5595	5588	17 869	σ	*M*	Γ_6^c
5509	5500	18 160	σ	*W*	
5432	5427	18 410	$st\sigma,\pi$	VS	Γ_6
5396	5413	18 500	σ	VW	
5370	5362	18 630	σ	VW,*sh*	

TABLE I. (*Continued*).

λ(Å) Conc. crystal	λ(Å) Diluted crystal	Energy (cm^{-1})	Polarization	intensity[a]	Assigned representation
5343	5337	18 720	σ,π	*W*	
5324		18 780	σ,π	*sh*	
5285		18 916	π	VW	
5248	5250	19 045	σ,π weak	*M*	Γ_6
5168	5161	19 350	$\sigma,st\pi$	*S*	Γ_7[c]
5137		19 460	σ	VW	
5096	5090	19 630	σ,π	*S*	Γ_6[c]
5073	5066	19 715	π	*sh*	
5030	5019	19 895	π	*M*	Γ_7
5018	5014	19 930	σ	*S*	Γ_6
4943	4939	20 230	σ	*M*	
4885	4883	20 470	σ	*S*	Γ_6
4859	4857	20 580	σ	*sh*	
4822	4826	20 730	π	*W*	
4815	4815	20 762	σ	VW	
4752	4750	21 038	π	*M*	
4743	one	21 078	σ	VW	
4730	broad	21 135	σ	*sh*	
4683	line	21 347	π	VW	
4601		21 728	σ	*M*	Γ_6
4579	4592	21 847	σ,π	*S*	Γ_7
4482	4479	22 310	σ,π	VW	
4431	4429	22 567	π	*M*	Γ_7
4424		22 598	σ	VW	
4350	4343	22 999	σ	VS	
4332	4323	23 100	π	VW	Γ_7
4291	4284	23 320	σ	*S*	b
4270		23 413	σ	*sh*	
4210	4201	23 760	π,σ weak	*W*	Γ_7
4177	4170	23 930	σ,π	*M*	Γ_7
4135		24 177	σ	VW	
4092		24 431	σ	VW	
3777	3769	24 490	σ	*M*	
3759	3759	26 595	σ	*sh*	
3530		28 320	σ	*W*	
3474		28 777	σ	*W*	

[a]VS, very strong; *S*, strong; *M*, medium; *W*, weak; VW, very weak; *sh*, shoulder.
[b]These transitions were not assigned.
[c]These transitions were assigned but not used in the fitting procedure.

C. Third group (9600–12 600 cm^{-1}, 10 500–7900 Å) (Fig. 1)

According to preliminary calculations (See Sec. IV A), the $J=\frac{13}{2},\frac{9}{2}$ (II), and $\frac{5}{2}$ (I) manifolds are expected to be found in this group. At this point, however, it was difficult to classify the individual *J* states for the 14 absorption bands detected in this range. Nine lines in this region could be identified as Γ_6 or Γ_7 crystal-field levels according to their polarization characteristics. As in the case of the first group, a weak, broad line at 9660 cm^{-1} was found at room temperature only about 350 cm^{-1} from the next intense transition. This temperature-dependent line confirmed the assignment of the first excited Γ_6 state at 350 cm^{-1}.

D. Fourth group (13 200–16 085 cm^{-1}, 7800–6100 Å) (Fig. 2)

A difference of only 650 cm^{-1} separated this group from the third group of transitions. Because of *J* mixing by the crystal field, some overlap may occur between this group and the lower energy one. Nevertheless, assuming that the *J* levels are relatively isolated, levels derived from the $J=\frac{5}{2}$ (II), $\frac{3}{2}$ (II), $\frac{7}{2}$ (I), and $\frac{15}{2}$ (I) are expected. Nine of the observed 14 bands in this group could be assigned from their polarization characteristics.

E. Fifth group (16 495–16 640 cm^{-1}, ~6000 Å)(Fig. 2)

Only two transitions appeared in this group that were separated from the other groups. As in other compounds

of Np^{4+}, these transitions can be attributed to the $^4G_{7/2}$ manifold. One transition is strongly π polarized (Γ_7) and the other is strongly σ polarized (Γ_6).

F. Sixth group (17 600–28 800 cm^{-1}, 5800–3500 Å) (Fig. 2)

This group represents the highest-energy part of the spectrum and was relatively complex. Fourteen intense lines could be identified as Γ_6 or Γ_7, however, from their strongly polarized transitions.

IV. OPTICAL DATA ANALYSIS

A. Energy level assignments

The energy levels within an f^n configuration in D_{2d} symmetry can be written in terms of the free-ion (H_{FI}) and crystal-field (H_{CF}) Hamiltonians as follows:[19–21]

$$H_{FI}=\sum_{k=0,2,4,6}F^k(nf,nf)f_k+\zeta_f a_{s.o.}+\alpha L(L+1)+\beta G(G_2)+\gamma(R_7)+\sum_{\substack{k=2,8\\k\neq 5}}T^k t_k+\sum_{k=0,2,4}M^k m_k+\sum_{k=2,4,6}P^k p_k\ , \tag{2}$$

and

$$H_{CF}=B_0^2C_0^2+B_0^4C_0^4+B_4^4(C_4^4+C_{-4}^4)+B_0^6C_0^6+B_4^6(C_4^6+C_{-4}^6)\ . \tag{3}$$

The $F^k(nf,nf)$'s and ζ_f above represent the radial parts of the electrostatic and spin-orbit interactions, respectively, between f electrons, while f_k and $a_{s.o.}$ are angular parts of these interactions. The parameters α,β, and γ are associated with the two-body effective operators of the configuration interaction and the T^k are the corresponding parameters of the three-body configuration interaction operators. The M^k parameters represent the spin-spin and spin-other-orbit interactions while the P^k parameters arise from electrostatic-spin-orbit interactions with higher configurations. The crystal-field interaction for D_{2d} symmetry is parametrized by B_0^2,B_0^4,B_4^4,B_0^6, and B_4^6, and the angular operators $C_q^{(k)}$ are the usual Racah tensors.

A preliminary calculation was performed using the free-ion parameters obtained from the analysis of the optical results of either Np^{4+}:$Zr(BD_4)_4$,[6] or Np^{4+}:$ThSiO_4$ (Ref. 7) along with the crystal-field parameters obtained from the analysis of the data for U^{4+}:$ZrSiO_4$. These calculations predicted a Γ_6 ground state that is well separated from the higher energy levels as well as relatively isolated J levels for those whose energy was less than ~ 10000 cm^{-1}.

B. Parametric fit of the optical data

From the calculated energy levels, 30 transitions could be assigned with good agreement between the calculated and measured energies, the consistency of the polarization characteristics, and the expected eigenvector composition. The free-ion parameters F^2,F^4,F^6, and ζ were varied with the crystal-field parameters fixed at the U^{4+}:$ZrSiO_4$ values. The crystal-field parameters were then allowed to vary with the free-ion parameters fixed, and finally, all of the above parameters were varied simultaneously. The remaining parameters were fixed at the values used for Np^{4+}:$Zr(BD_4)_4$. For the fit with 31 levels, an rms deviation of 34 cm^{-1} was obtained.

Thirteen additional transitions were present that, together with the 30 transitions discussed above, correspond to the strongest observed transitions. The addition of these 13 transitions resulted in some interchanges in the Γ_6 and Γ_7 levels in the calculated spectrum. Furthermore, fitting these additional levels did not improve the rms deviation obtained by using the parameters resulting from the 31 level fit when the extra 13 transitions were assigned to the nearest calculated energy level of the correct symmetry.

The final values of the parameters obtained with the 31 level fit are given in Table II and this fit resulted in an rms deviation of $\sigma=34$ cm^{-1} as noted above (varying 12 parameters including α and β). For the fit with 44 levels a value for σ of 103 cm^{-1} was obtained. The calculated energy levels and eigenvectors are given in Table III.

TABLE II. Final parameter values of Np^{4+}:$ZrSiO_4$ (all parameters in cm^{-1}).

F^2	47 479(221)
F^4	41 455(442)
F^6	26 528(353)
α	392(1.9)
β	−611(76)
γ	[1200][a]
T^2	[278]
T^3	[44]
T^4	[64]
T^6	[−361]
T^7	[434]
T^8	[353]
ζ	2088(4)
M^0	[0.88]
M^2	[0.49]
M^4	[0.34]
P^2	[500]
P^4	[500]
P^6	[500]
B_0^2	−2537(101)
B_0^4	2304(208)
B_4^4	−5281(149)
B_0^6	−5065(150)
B_4^6	642(125)
n[b]	31 {44}
σ[c]	33 {103}

[a]Values of the parameters in [ ] are fixed as in Ref. 6.

[b]n is the number of levels; values in { } are for 44 assigned levels with the above parameters.

[c]$\sigma=(\sum(E_{calc}-E_{expt})^2/n-p)^{1/2}$ where E_{calc} and E_{expt} are the calculated and experimental energies and p is the number of free parameters.

TABLE III. Calculated and experimental energy levels.

Γ	E_{calc} (cm^{-1})	E_{obs} (cm^{-1})	ΔE (cm^{-1})	Eigenvector
6	0	0	0	84.1% $^4I_{9/2}$ + 11.7% $^2H_{9/2}(2)$
6	363.8	350.0	13.8	79.8% $I_{9/2}$ + 13.3% $^2H_{9/2}(2)$
7	557.8			80.1% $^4I_{9/2}$ + 13.4% $^2H_{9/2}(2)$
6	831.1			78.6% $^4I_{9/2}$ + 14.5% $^2H_{9/2}(2)$
7	1374.5			76.7% $^4I_{9/2}$ + 16.9% $^2H_{9/2}(2)$
7	5500.1	5514.0	−13.9	80.4% $^4I_{11/2}$ + 6.9% $^4F_{3/2}$
6	5704.3	5723.0	−18.7	92.2% $^4I_{11/2}$ + 3.3% $^8H_{11/2}(2)$
6	6066.9	6056.0	10.9	88.2% $^4I_{11/2}$ + 4.1% $^2H_{11/2}(2)$
7	6067.7	6072.0	−4.3	85.8% $^4I_{11/2}$ + 3.8% $^2H_{11/2}(2)$
6	6466.5	6468.0	−1.5	88.5% $^4H_{11/2}$ + 4.1% $^2H_{11/2}(2)$
7	6496.3	6496.0	0.3	89.2% $^4I_{11/2}$ + 4.6% $^2H_{11/2}(2)$
7	8286.0	8310.0	−24.0	44.8% $^4F_{3/2}$ + 16.5% $^2D_{3/2}(1)$
6	8408.7	8366.0	42.7	55.5% $^4F_{3/2}$ + 21.0% $^2D_{3/2}(1)$
6	10 060.0	10 016.0	44.0	80.9% $^4I_{13/2}$ + 5.3% $^2K_{13/2}$
7	10 070.4	10 062.0	8.4	74.5% $^4I_{13/2}$ + 5.8% $^2K_{13/2}$
7	10 529.0	10 450.0	79.0[a]	78.1% $^4I_{13/2}$ + 4.5% $^2K_{13/2}$
7	10 583.9			70.0% $^4I_{13/2}$ + 11.4% $^4F_{5/2}$
6	10 748.0			66.6% $^4I_{13/2}$ + 5.8% $^4F_{9/2}$
7	11 035.3	10 896.0	139.3[a]	66.4% $^4I_{13/2}$ + 6.7% $^4F_{5/2}$
6	11 231.7	11 147.0	84.7[a]	28.5% $^4I_{13/2}$ + 11.0% $^4F_{5/2}$
6	11 299.7	11 571.0	−271.3[a]	73.1% $^4I_{13/2}$ + 9.0% $^4F_{5/2}$
7	11 315.3			12.5% $^4I_{13/2}$ + 11.7% $^2H_{9/2}(2)$
6	11 891.8	11 935.0	−43.2	21.3% $^4F_{5/2}$ + 15.5% $^2G_{9/2}(1)$
7	11 940.6			19.5% $^2H_{9/2}(2)$ + 14.6% $^2G_{9/2}(1)$
7	12 211.6	12 196.0	15.6	34.6% $^4F_{5/2}$ + 15.9% $^4G_{5/2}$
7	12 334.4			45.8% $^4F_{5/2}$ + 8.6% $^4I_{13/2}$
6	12 367.6			23.6% $^4F_{5/2}$ + 15.0% $^4G_{5/2}$
6	12 569.6	12 537.0	32.6	29.7% $^2H_{9/2}(2)$ + 18.0% $^2G_{9/2}(1)$
7	13 010.2			63.7% $^4G_{5/2}$ + 7.8% $^4F_{3/2}$
6	13 158.2	13 188.0	−29.8	36.5% $^4S_{3/2}$ + 17.5% $^4I_{15/2}$
7	13 362.0	13 352.0	10.0	22.4% $^4S_{3/2}$ + 16.9% $^4F_{5/2}$
6	13 594.1			30.3% $^4F_{7/2}$ + 13.1% $^4F_{5/2}$
7	14 027.4	13 861.0	166.4[a]	24.3% $^4F_{7/2}$ + 7.9% $^4F_{5/2}$
6	14 296.8	14 036.0	260.8[a]	42.6% $^4F_{15/2}$ + 20.0% $^4S_{3/2}$
7	14 326.2	14 158.0	168.2[a]	60.2% $^4I_{15/2}$ + 12.7% $^2K_{15/2}$
6	14 429.0			26.7% $^4G_{5/2}$ + 16.7% $^4F_{5/2}$
7	14 598.4	14 555.0	43.4	65.9% $^4I_{15/2}$ + 10.2% $^2K_{15/2}$
7	14 865.7			25.7% $^4F_{7/2}$ + 19.4% $^4I_{15/2}$
6	14 901.3			37.3% $^4F_{7/2}$ + 22.2% $^4G_{5/2}$
7	14 997.4	15 014.0	−16.6	29.0% $^4I_{15/2}$ + 23.5% $^4G_{5/2}$
7	15 286.8			37.9% $^4I_{15/2}$ + 23.3% $^4F_{7/2}$
6	15 578.8			64.8% $^4I_{15/2}$ + 9.5% $^2K_{15/2}$
7	15 636.4	15 983.0	−346.6[a]	60.0% $^4I_{15/2}$ + 15.5% $^2K_{15/2}$
6	15 697.8			67.6% $^4I_{15/2}$ + 13.0% $^2K_{15/2}$
6	15 872.1	16 025.0	−138.9[a]	53.4% $^4I_{15/2}$ + 12.1% $^2K_{15/2}$
7	16 466.8	16 495.0	−28.2	60.6% $^4G_{7/2}$ + 11.5% $^4F_{7/2}$
6	16 542.7	16 640.0	97.3[a]	55.2% $^4G_{7/2}$ + 9.0% $^4F_{7/2}$
7	17 002.0			57.7% $^4G_{7/2}$ + 14.9% $^4F_{7/2}$
6	17 227.0			55.2% $^4G_{7/2}$ + 19.1% $^4F_{7/2}$
16	17 814.4	17 869.0	−54.6[a]	43.6% $^4F_{3/2}$ + 12.3% $^2H_{9/2}(2)$
7	17 962.8			43.0% $^4F_{9/2}$ + 11.4% $^2H_{9/2}(2)$
6	18 207.0			42.0% $^4F_{9/2}$ + 17.7% $^2H_{9/2}(2)$
6	18 436.1	18 410.0	26.1	26.0% $^4F_{9/2}$ + 23.1% $^2K_{13/2}$
7	18 778.9			21.4% $^2K_{13/2}$ + 18.1% $^2H_{11/2}(2)$
7	18 805.8			26.9% $^2K_{13/2}$ + 19.5% $^4F_{9/2}$
6	18 832.7			32.0% $^2H_{11/2}(2)$ + 18.3% $^4G_{11/2}$
6	19 002.2	19 045.0	−42.8	21.6% $^4F_{9/2}$ + 13.3% $^2H_{11/2}(2)$
7	19 021.5			31.4% $^2K_{13/2}$ + 23.2% $^4F_{9/2}$
6	19 173.6			30.2% $^2K_{13/2}$ + 15.4% $^4F_{9/2}$

TABLE III. (*Continued*).

Γ	E_{calc} (cm^{-1})	E_{obs} (cm^{-1})	ΔE (cm^{-1})	Eigenvector
7	19485.0	19350.0	135.0[a]	27.3% $^2H_{11/2}(2)$ + 22.5% $^2K_{13/2}$
6	19542.8	19630.0	−87.2[a]	22.2% $^2H_{11/2}(2)$ + 20.5% $^2K_{13/2}$
7	19874.8	19895.0	−20.2	51.6% $^2H_{11/2}(2)$ + 19.7% $^4G_{11/2}$
6	19908.4	19930.0	−21.6	39.4% $^2H_{11/2}(2)$ + 17.1% $^4G_{11/2}$
6	20028.8			15.1% $^2K_{13/2}$ + 13.8% $^2H_{11/2}(2)$
7	20063.5			37.0% $^2K_{13/2}$ + 19.8% $^2H_{11/2}(2)$
7	20162.3			26.7% $^2K_{13/2}$ + 7.7% $^4S_{3/2}$
7	20382.7			30.7% $^2H_{11/2}(2)$ + 22.7% $^2K_{13/2}$
6	20513.3	20470.0	43.3	20.5% $^4D_{1/2}$ + 17.2% $^2P_{1/2}$
7	20537.0			58.7% $^2K_{13/2}$ + 8.3% $^2G_{7/2}(1)$
6	20808.4			49.0% $^2K_{13/2}$ + 9.3% $^4G_{9/2}$
7	20852.3			48.7% $^4G_{9/2}$ + 11.3% $^4D_{5/2}$
6	20970.8			26.2% $^4G_{9/2}$ + 14.1% $^2P_{1/2}$
6	21203.8			45.7% $^4G_{9/2}$ + 7.8% $^4D_{5/2}$
6	21369.7			29.0% $^4G_{9/2}$ + 10.0% $^4D_{5/2}$
7	21422.8			55.4% $^4G_{9/2}$ + 6.5% $^2H_{9/2}(1)$
6	21714.0	21728.0	−14.0	34.8% $^4G_{9/2}$ + 15.9% $^2G_{7/2}(1)$
7	21830.7	21847.0	−16.3	33.7% $^4D_{5/2}$ + 20.2% $^2D_{5/2}(2)$
7	21873.5			28.1% $^2K_{13/2}$ + 15.2% $^2G_{7/2}(1)$
6	22084.2			26.3% $^4G_{9/2}$ + 12.0% $^2G_{7/2}(1)$
7	22289.9			30.8% $^2K_{13/2}$ + 15.9% $^2G_{7/2}(1)$
6	22451.8			29.4% $^4G_{9/2}$ + 16.9% $^4D_{5/2}$
7	22595.8	22567.0	28.8	21.1% $^4D_{5/2}$ + 17.0% $^2D_{5/2}(2)$
6	23106.8			22.0% $^2K_{15/2}$ + 16.8% $^2L_{15/2}$
7	23130.2	23100.0	30.2	22.8% $^2K_{15/2}$ + 19.0% $^2L_{15/2}$
7	23280.5			29.2% $^2L_{15/2}$ + 27.3% $^2K_{15/2}$
6	23734.6			25.9% $^2L_{15/2}$ + 18.6% $^2K_{15/2}$
7	23772.2	23760.0	12.2	20.9% $^4D_{3/2}$ + 12.0% $^2D_{3/2}(1)$
7	23888.6	23930.0	−41.4	24.1% $^2K_{15/2}$ + 18.4% $^2L_{15/2}$
6	23900.7			22.2% $^2H_{11/2}(1)$ + 13.8% $^2L_{15/2}$
6	24101.4			19.3% $^2L_{15/2}$ + 17.4% $^2K_{15/2}$
6	24331.7			17.2% $^4D_{3/2}$ + 13.9% $^2K_{15/2}$
7	24406.9			24.6% $^2H_{11/2}(1)$ + 11.7% $^2D_{5/2}(1)$
6	24652.3			37.7% $^2H_{11/2}(1)$ + 12.4% $^2I_{11/2}$
7	24672.6			15.4% $^2D_{5/2}(1)$ + 13.6% $^2K_{15/2}$
7	24715.0			25.6% $^2K_{15/2}$ + 17.4% $^2L_{15/2}$
6	24827.3			35.1% $^2K_{15/2}$ + 25.3% $^2L_{15/2}$
6	24921.3			43.3% $^2H_{11/2}(1)$ + 22.7% $^4G_{11/2}$
7	25005.4			52.9% $^2D_{5/2}(1)$ + 13.2% $^2H_{11/2}(1)$
7	25205.1			36.8% $^2H_{11/2}(1)$ + 17.6% $^4G_{11/2}$
6	25893.4			21.8% $^4G_{11/2}$ + 14.1% $^2D_{5/2}(1)$

[a]These thirteen levels were assigned but were not used in the fitting procedure. See text.

V. EPR GROUND-STATE DATA AND ANALYSIS

The EPR line positions obtained as a function of the applied magnetic-field orientation were fitted to the parameters of the axial spin Hamiltonian[22]

$$\mathcal{H}=g_{\parallel}\mu_B H_z S_z + g_{\perp}\mu_B (H_x S_x + H_y S_y) + A S_z I_z + B(S_x I_x + S_y I_y) , \quad (4)$$

where μ_B is the Bohr magneton and H is the magnetic field. The other parameters have their usual meaning. Due to the small value of $g_{\parallel}$ and the problems with the orientation of the crystal, the uncertainties in the values of $g_{\parallel}$ and A are much greater than the errors in $g_{\perp}$ and B. The resulting parameters for the spin Hamiltonian are given in Table IV. An additional analysis was attempted in which a quadrupolar term was added to the spin Hamiltonian, but this refinement did not significantly improve

TABLE IV. Spin-Hamiltonian parameters for Np^{4+}:$ZrSiO_4$.

	EPR	Optical[a]
$\lvert g_{\parallel} \rvert$	0.8±0.6	−0.1
$\lvert g_{\perp} \rvert$	2.59±0.02	2.9
A(MHz)	−2400±1200	
B(MHz)	4750±30	

[a]Calculated from the wave functions obtained from fitting the optical spectra.

TABLE V. Ratios of the hyperfine coupling constants and g values.

Compound	$\frac{a}{g}$ or $\frac{B}{g_\perp}$	Ref.
Np^{4+}:Cs_2ZrCl_6	1848±60	23
$Np(BH_4)_4$:$Zr(BH_4)_4$	1807	6
$Np(BH_3CH_3)_4$:$Zr(BH_3CH_3)_4$	1869	6
Np^{4+}:$ZrSiO_4$	1834	This work

the fit. The data given in Table IV are consistent with the calculated Γ_6 calculated ground state and serve to confirm that assignment.

For a pure J state, the ratio of a/g, $A/g_\parallel$, and $B/g_\perp$ should be constant, (where a and g are, respectively, the hyperfine coupling constant and g value of a particular J manifold of the free ion). There are two other reported measurements for Np^{4+} in various crystals or molecules,[6,23] and these ratios are given in Table V along with the present value obtained for Np^{4+} in $ZrSiO_4$. The ground-state wave function obtained from the optical fit shows that the ground state is $\sim 97\%$ pure $J=\frac{9}{2}$. Therefore, this ratio should represent a check on the validity of the present data. The agreement between the earlier a/g ratios and the $B/g_\perp$ value obtained in this work are considered to be satisfactory. The experimental uncertainties in A and $g_\parallel$, however, are too great to apply this test.

VI. DISCUSSION

The parameters for those actinide ions in $ZrSiO_4$ and $ThSiO_4$ whose optical spectra have been analyzed are listed in Table VI. It is reassuring to note that the crystal-field parameters for U^{4+}:$ZrSiO_4$ and Np^{4+}:$ZrSiO_4$ are very similar. The crystal-field parameters for Np^{4+}:$ZrSiO_4$ are quite different and much larger than those for Np^{4+}:$ThSiO_4$. A qualitative measure of the magnitude of the crystal field is given by the Auzel parameter $[N_v/(4\pi)^{1/2}]$ (Ref. 24) which is also listed in Table VI.

For f^n ions where n is odd, the selection rules are not very restrictive. The present analysis is essentially based on crystal-field parameters obtained from the U^4:$ZrSiO_4$ analysis. With the use of these parameters and the Np^{4+} free-ion parameters resulting from the Np^{4+}:$Zr(BD_4)_4$ analysis, it was possible to assign 31 Np^{4+} energy levels rather easily, and adjustment of the parameters as described earlier led to a very good value for σ. It is rather disturbing, however, that 13 other transitions of comparable intensity and with good polarization characteristics led to an increased rms deviation of $\sim 100\ cm^{-1}$.

The reason for the above discrepancy is not understood at present. The absorption lines were very broad, and the line width did not decrease markedly in the dilute crystal. It is possible that more than one Np site is present in these crystals that could be responsible for the observed large line widths and the noted marked deviations in the

TABLE VI. Comparison of U^{4+} and Np^{4+} parameters in different silicates.

	U^{4+}:$ThSiO_4$[a]	U^{4+}:$ZrSiO_4$[b]	Np^{4+}:$ThSiO_4$[c,d]	Np^{4+}:$ZrSiO_4$[d]
F^2[e]	43 110(245)	44 258	45 196(716)	47 479[221]
F^4[e]	40 929(199)	40 293	38 032(546)	41 455[442]
F^6[e]	23 834(639)	31 287	28 343(791)	26 528[353]
ζ[e]	1840(2)	1740	2129(7)	2088[4]
α[e]	32.3(0.4)	23	15(3)	39.2[1.9]
β[e]	−663(144)		[−600]	−610(76)
γ[e]	[1200]		[1200]	[1200]
B_0^2[e]	−1003(127)	−2000	323(185)	−2537(101)
B_0^4[e]	1147(281)	2000	1511(278)	2304(208)
B_4^4[e]	−2698(251)	−5125	−3559(163)	−5281(149)
B_0^6[e]	−2889(557)	−5792	−1871(372)	−5065(150)
B_4^6[e]	−208(333)	427	−801(197)	642(125)
n	25	30	29	31 (44)
σ[e]	71	112	47	34 (103)
$\frac{F^2_{cry}}{F^2_{FI}}$	0.83	0.85	0.83	0.87
$\frac{\zeta_{cry}}{\zeta_{FI}}$	0.93	0.88	0.94	0.93
$\frac{F^4_{cry}}{F^2_{cry}}$	0.95	0.91	0.84	0.87
$\frac{N_v}{(4\pi)^{1/2}}$[e]	1617	3113	1859	3179

[a]Reference 14.
[b]Reference 13.
[c]Reference 7.
[d]The T^k,M^k, and P^k values are given in Table II.
[e]In cm^{-1}.

fit for some levels. Additionally, impurities can arise from the flux used in the crystal-growth process. Unfortunately, however, it is difficult to explore a variety of growth conditions when radioactive materials are employed.

Although the free-ion parameters for Np^{4+}:$ZrSiO_4$ were obtained over a small energy range and must be considered to be rather tentative, the ratios of the parameters given in Table VI, as defined by Rajnak *et al.*,[6] are consistent with the observations in that work. All of the Np^{4+}:$ZrSiO_4$ ratios indicate decreasing covalency with increasing atomic number as compared to the results for U^{4+} in $ZrSiO_4$. It should be noted, however, that there is increased scatter when the corresponding ratios are compared for U^{4+} and Np^{4+} in the $ThSiO_4$ host.

VII. CONCLUSION

The optical spectrum of Np^{4+}:$ZrSiO_4$ has been analyzed with 31 strong transitions assigned using crystal-field parameters consistent with those determined previously for U^{4+}:$ZrSiO_4$. Thirteen other relatively intense levels did not fit well. EPR results confirmed the assignment of the ground crystal-field state of Np^{4+} in $ZrSiO_4$. A comparison of the empirical parameters obtained for Np^{4+}:$ZrSiO_4$ with those obtained for the U^{4+}:$ZrSiO_4$ shows the same trends as those found in comparing the parameters of Np^{4+}:$Zr(BD_4)_4$ with those of U^{4+}:$Hf(BD_4)_4$ (Refs. 6 and 25) i.e., covalency effects are found to decrease with increasing atomic number.

ACKNOWLEDGMENTS

This work was supported by the Director, Office of Energy Research, Office of Basic Energy Sciences, Chemical Sciences Division of the U.S. Department of Energy under Contract No. DE-AC03-76SF00098 and by the Division of Materials Science, U.S. Department of Energy, under Contract No. DE-AC05-84OR21400 with Martin Marietta Energy Systems, Inc. We wish to thank Ray Gatti for help with the gamma-ray counting experiments, Glen Williams and David Piehler for the electronic Raman and fluorescence experiments, and Homer Harmon for his technical assistance during the growth of these radioactive materials. The authors are also indebted to John Bigelow and other staff members of the transuranium element production facilities at the Oak Ridge National Laboratory.

[1]J. P. Hessler and W. T. Carnall in *Lanthanide and Actinide Chemistry and Spectroscopy,* Vol. 131 of the American Chemical Society Symposium Series, 131, edited by N. Edelstein, (American Chemical Society, Washington, D.C., 1980), p. 349.

[2]N. Edelstein, J. Less-Common Met. **133**, 39 (1987); C. D. Flint and P. A. Tanner, Mol. Phys. **61**, 389 (1987).

[3]J. B. Gruber and E. R. Menzel, J. Chem. Phys. **50**, 3772 (1969).

[4]K. K. Sharma and J. O. Ortman, J. Chem. Phys. **50**, 1241 (1969).

[5]E. R. Menzel and J. B. Gruber, J. Chem. Phys. **54**, 3857 (1971).

[6]K. Rajnak, R. H. Banks, E. Gamp, and N. Edelstein, J. Chem. Phys. **80**, 5951 (1984).

[7]M. P. Lahalle, J. C. Krupa, and R. Guillaumont, J. Less-Common Met. **122**, 65 (1986).

[8]R. W. Wyckoff, *Crystal Structures,* 2nd Ed. (Interscience, New York, 1965), Vol. 3, p. 15.

[9]R. W. Reynolds, L. A. Boatner, C. B. Finch, A. Chatelain, and M. M. Abraham, J. Chem. Phys. **56**, 5607 (1972).

[10]Vishwamittar and S. P. Puri, Phys. Rev. B **9**, 4673 (1974).

[11]R. D. Shannon, Acta Cryst. A **32**, 751 (1976).

[12]D. J. Mackey, W. A. Runciman, and E. R. Vance, Phys. Rev. B **11**, 211 (1975).

[13]E. R. Vance, D. J. Mackey, Phys. Rev. B **18**, 185 (1978).

[14]C. Khan Malek, J. C. Krupa, P. Delamoye, and M. Genet, J. Less-Common Met. **122**, 75 (1986).

[15]A. A. Ballman and R. A. Laudise, J. Amer. Ceram. Soc. **48**, 130 (1965).

[16]A. B. Chase and J. A. Osmer, J. Electrochem. Soc. **113**, 198 (1966).

[17]D. Ball and B. M. Wanklyn, Phys. Status Solidi A **36**, 307 (1976).

[18]G. F. Koster, J. O. Dimmock, R. G. Wheeler, and H. Statz, *Properties of the Thirty-Two Point Groups* (M.I.T. Press, Cambridge, 1963).

[19]B. G. Wybourne, *Spectroscopic Properties of the Rare Earths* (Wiley, New York, 1965).

[20]B. R. Judd, *Operator Techniques in Atomic Spectroscopy* (McGraw-Hill, New York, 1963).

[21]W. T. Carnall, H. Crosswhite, and H. M. Crosswhite, J. P. Henla, N. M. Edelstein, J. G. Conway, G. V. Shalimoff, and R. Sarup, J. Chem. Phys. **72**, 5089 (1980).

[22]A. Abragam and B. Bleaney, *Electron Paramagnetic Resonance of Transitions Ions* (Clarendon, Oxford, 1970).

[23]N. Edelstein, W. Kolbe, and J. E. Bray, Phys. Rev. B **21**, 338 (1980).

[24]F. Auzel and O. L. Malta, J. Phys. (Paris) **44**, 201 (1983).

[25]K. Rajnak, E. Gamp, R. Shinomoto, and N. Edelstein, J. Chem. Phys. **80**, 5942 (1984).